Journal of King Saud University – Science 34 (2022) 101894

Contents lists available at ScienceDirect

Journal of King Saud University – Science

journal homepage: www.sciencedirect.com

Original article

Two-step chromium photo-precipitation in the sequential UV/Sulfite/Manganese dioxide processes: Efficiency, kinetic, energy-economic evaluation, and sludge survey

Shohreh Azizi [a,b], Maryam Sarkhosh [c,e,a,b,*], Ilunga Kamika [d], Thabo Nkambule [d], Malik Maaza [a,b]

[a] UNESCO-UNISA Africa Chair in Nanosciences and Nanotechnology, College of Graduate Studies, University of South Africa, Muckleneuk Ridge, PO Box 392, Pretoria 0002, South Africa
[b] Nanosciences African Network (NANOAFNET), iThemba LABS-National Research Foundation, 1 Old Faure Road, Somerset West 7129, PO Box 722, Somerset West, Western Cape 7131, South Africa
[c] Social Determinants of Health Research Center, Mashhad University of Medical Sciences, Mashhad, Iran
[d] Institute for Nanotechnology and Water Sustainability, School of Science, College of Science, Engineering and Technology, University of South Africa, Florida Campus, Johannesburg, South Africa
[e] Department of Environmental Health Engineering, School of Health, Mashhad University of Medical Sciences, Iran

ARTICLE INFO

Article history:
Received 21 November 2021
Revised 26 January 2022
Accepted 4 February 2022
Available online 9 February 2022

Keywords:
Chromium
Concern
Reduction
Photo-sedimentation
Real sample
Radicals

ABSTRACT

In this study, removal of Chromium (Cr) in a novel process includes reduction, adsorption, oxidation and complexion in a UV/Sulfite/Manganese dioxide (USM) investigated. In our study, in the optimal condition was MnO_2 = 1 mM, Na_2SO_3 = 0.4 mM, 6 min reaction time (synthetic sample) and at pH 7, and 10 mg L^{-1} Cr removed completely. In the first stage, the sulfite-sulfate radicals react with Cr, and then Cr-S are removed from the solution by forming a complex with $MnOOH^{\cdot}$. Advantage of this method against other process include less time, higher efficiency, less use of reactive materials, and no need for large pH changes without release of sulfite or sulfate. At pH 7 about 60% and 40% of reaction species were reduction and oxidative species respectively. Considering the better efficiency at pH 7, it shows that reducing species have a more important and primary role in Cr removal. Also, the amount of energy consumed decreases from 16.14 to 3.25 kWh per cubic meter, K_{obs} (min^{-1}) 0.533to 0.1837 and r_{obs} (mg/L.min) increase from 26.68 to 45.2 with change of Cr concentration from 50 to 250 mg L^{-1} respectively. The total cost of the USM process is much lower than other methods. In the UV, U Manganese dioxide, UV/Sulfite, and USM methods, the total cost were estimated 9.80–18.75, 5.74–8.75, 5.72–1.51, and 2.74–0.55 $ when the Cr concentration increase 100 to 250 mg L^{-1}, respectively.

1. Introduction

The presence of heavy metals in water due to its high toxicity and non-degradability by microorganisms and their high depletion in water resources, has created many risks to the environment and human health (Ding et al., 2021). Chromium (Cr) is one of the main mineral water pollutants in aqueous media, that hexavalent Cr has high solubility and toxicity compared to trivalent Cr and can be very dangerous to humans due to mutagenicity, teratogenicity and carcinogenicity (Liu and Yu 2021). Increasing the use of chromium in the chemical industry, metal plating, tanning and leather dyeing processes, and discharging their wastewater into the aqueous medium has increased the concentration of this pollutant in water sources (Ozcelik et al., 2021). To this end, the introduction of new methods to remove Cr from wastewater is crucial to protecting the environment and human health. Various methods including chemical sedimentation (Harper and Kingham 1992), adsorption (Liu et al., 2020; Sadani et al., 2020), ion exchange (Lee et al., 2017), electrochemical treatment (Syam Babu and Nidheesh 2021), and membrane (Hao et al., 2018), advanced treatment processes (ATPs) (Babu et al., 2019) technologies for separation of chromium from contaminated water have been proposed. Advanced Treatment Processes (ATP) are able to achieve removal of specific organic and inorganic ingredients in solution, which

* Corresponding author at: Social Determinants of Health Research Center, Mashhad University of Medical Sciences, Mashhad, Iran.
E-mail addresses: azizis@unisa.ac.za (S. Azizi), Marya.sarkhosh@yahoo.com (M. Sarkhosh), Kamiki@unisa.ac.za (I. Kamika), nkambtt@unisa.ac.za (T. Nkambule).
Peer review under responsibility of King Saud University.

Production and hosting by Elsevier

https://doi.org/10.1016/j.jksus.2022.101894
1018-3647/

are not normally achieved by other treatment options (Rasolevandia et al., 2020) Inorganic anions such as Iodide (Rasolevandia et al., 2020), Sulfite (Sarkhosh et al., 2019), and Carboxylates (Massoudinejad et al., 2020) are stimulated to produce electrons and reducing species when exposed to a UV activator. In the last decade, a new advanced reduction process has been developed and patented using soluble sulfur (IV) (sulfite) as the photo absorber to produce large amounts of electrons (e^-_{aq}) (Zaw and Emett 2002; Azarpira et al., 2019). In this study Sulfite chosen due to two very important properties: UV absorption and electron production per photon are absorbed, which in sulfite are 253.7 nm (εi, 254 = 220 M^{-1} cm^{-1}, respectively), and e^-_{aq} (eg, 0.286 mol E^{-1}). Manganese oxide has been widely studied as one of the most important oxidizing agents for oxidation due to its strong oxidation ability and strong stability. In this study UV_{254} rays was used to stimulate sulfite and Manganese dioxide ions to create both regenerative species or react directly with pollutants. Therefore, in this study, UV rays were used to stimulate sulfite and remove direct and indirect chromium in photo reactor.

2. Martial and methods

2.1. Reactor configuration

A UV lamp (nominal power: 11 W; light intensity: 78 μW/cm^2) with wavelength emission in the range λ_{max} = 254 nm was used as UV irradiation source with quartz sleeve fixed in center of the tubular glass (distance of 1 cm from the quartz). Arsenic solution was entered in the empty space between the quartz and tubular glass as reaction space. The experiments were performed in a 500 mL container. To prevent the effect of the lamp temperature on the reaction and disturbance in the results obtained, water was rotated around tubular glass.

2.2. Analytical methods

In As photo-sedimentation, the effects of initial Cr concentration (50 to 250 mg L^{-1}), initial pH (3 to 11) and photo-reaction time (0 to 50 min) were investigated. Graphite atomic absorption spectroscopy was used to measure the residual chromium concentration. The following equation was used to determine the photo-sedimentation of Cr.

$$\text{Arsenicphoto} - \text{sedimentation} = \frac{Cr_0 - Cr_t}{Cr_0} \quad (1)$$

Cr_0 and Cr_t are defined as the Cr concentration (mg L^{-1}) at the beginning and time of the reaction, respectively. Also the effect of anions on the photo-sedimentation of Cr was investigated.

2.3. Kinetic model, energy and effective cost analyses

Because it is almost impossible to determine the amount of reducing species in solutions, according to Eqs. (7)–(8), the Pseudo-first-order (PFO) was used to study the Cr reduction model.

$$ln\frac{C_t}{C_0} = -K_{obs} \quad (2)$$

$$r_{obs} = -k_{obs}C_{\text{Chromate}} \quad (3)$$

In this equation, k is the constant coefficient of reaction rate.

Important factors such as economy, wastewater quality, cost, etc. also play a key role in choosing a treatment technology. The major part of the cost of photo processes in the removal of water pollutants is related to electrical energy, electrical energy represents a major part of operating costs. Although there are several methods in determining the AORP electrical energy consumption in the literature and it depends on the type of pollutant, effluent quality, the reactor configuration and the type of light source used, etc., it is necessary to study the AORP electrical energy consumption under experimental conditions. The International Union of Pure and Applied Chemistry (IUPAC) has introduced the parameter of energy consume for each order (Figure-of-merit) that briefly called E_{EO} to determine the amount of electrical energy (kW·h) in UV-based reactions. Electrical energy per order E_{Eo} allows to quickly determine the electrical energy consumption and they show the total energy required. For the purpose of comparison, the treatment efficiency for different processes is evaluated through E_{Eo} values. This means that energy used to almost 90% of photo-remove contaminants in one cubic meter of contaminated water(Rasolevandi et al., 2019).

$$IUPACE_{\text{EO}} = \frac{P \times t \times 1000}{V \times 60 \times \log\frac{C_i}{C_f}} \quad (4)$$

In this equation, P is the amount of power (Kw), V is the volume (L), t is the photo-reaction time (minutes) of water in the photo-reactor. By combining and rearranging Eqs. (21) and (23), new E_{EO} obtains based on kinetic equation (Lee et al., 2018).

$$KineticE_{\text{EO}} = \frac{P \times 38.4}{V \times K_{obs}} \quad (5)$$

$$EEM = \frac{Pt}{VM \times (c_i - c_e)} \quad (6)$$

Where P is electrical power applied (kW) for the photoreactor, t refers to reaction time (h), M is the molar mass (g mol^{-1}) of C, V denotes the volume of Cd in inside reactor (L), c_i and c_e are the initial (or influent) and final (or effluent) concentrations of Cr. Also to calculate the total cost of the system (TCS) ($ g^{-1}), the following equation was applied (Xu et al., 2016a,b; Dhaka et al., 2018). In 2020, the world average of electricity prices is 0.121 U.S. Dollar per kWh for industrial users.

$$\begin{aligned}\text{TCS} = {} & 1.45\times(\text{EEM (kWh } g^{-1}) \times \text{ power cost (\$ /kWh)}) \\ & + Oxidantcost(\$g^{-1}) + Reductantcost(\$g^{-1})\end{aligned} \quad (7)$$

2.4. Reduction and oxidation species activity tests

The photocatalytic tests were carried out in UV-only, UV/Sulfite, UV/Manganese dioxide and there of them, in percent of Oxidative and reductive scavengers at the optimal condition. The initial concentration of Cr (III) was 50, 100 and 250 μg l^{-1}. To understand the role of $HO^{\cdot}$, h^+ and $O_2^{\cdot-}$ and reductive species in the mechanism of the Cr (III) removal, experiments with the addition of oxidative and reductive species scavengers including isopropyl alcohol, sodium oxalate and benzoquinone and nitrate (10 mL scavengers in 100 mL of Cr (III) aqueous solution) were performed(Gekko et al., 2012; Alam et al., 2019). For all tests, the reactor was in the dark for 1 h before the UV lamp was turned on. During the test, several samples were collected at constant time and the concentrations of Cr (III) and Cr (V) were analyzed.

3. Result and discussion

3.1. Effect of factors in Cr photo-sedimentation

3.1.1. Effect of pH

The effect of pH on Cr removal in UV/Manganese dioxide (UV/M), UV/Sulfite (US) and UV/Sulfite/Manganese dioxide USM were investigated over a wide pH range (3–11). Cr shown in Fig. 1, without irradiation, the removal of Cr (III) at pH 3 was significant (about

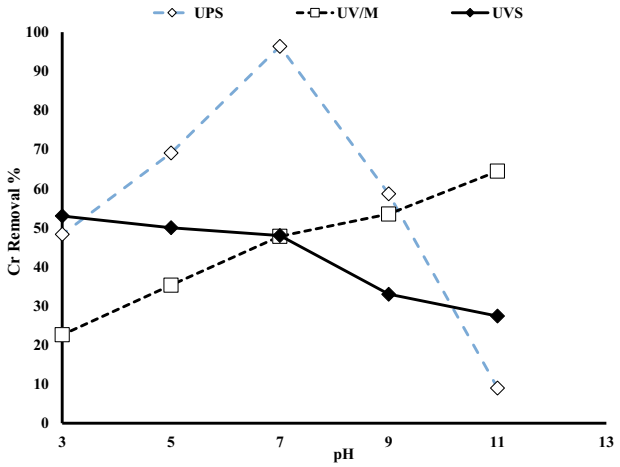

Fig. 1. Effect of pH on the removal of Cr (The experimental conditions: MnO_2:1 Mm, Sulfite: 0.4 Mm, Cr = 10 mg L^{-1}, 6 min reaction time).

20). It can be concluded that the adsorption rate of Cr by Manganese dioxide particles is 20%. The effect of the presence of sulfite is also different at various pH values shows that decreased with increasing pH. In the presence of sulfite, k_{obs} is significantly higher than that in the absence of sulfite over the whole pH range investigated (Xu et al., 2016a,b). In many researches, the rate of Cr removal increased in low pH level, which is consistent with the findings of our study (He et al., 2020; Kong et al., 2020; Kong et al., 2021). At pH > 3.1, the surface of MnO_2 negative charge while positive charge is corresponded to pH < 3.1. That's means in pH < 3.1, surface of MnO_2 prepare to complex with Cr-S (ALAH ABADI et al., 2021). Generation of hydrated electrons (e_{aq}^-) and hydrogen radicals (H·) in the stimulation of sulfite ions by UV which causes reduction of pH and release of Cr (V) in solution. Hexavalent chromium can react with SO_3^-· and SO_4—· radicals in the aqueous medium (Zhang et al., 2018), and then S-Cr can be react by the *MnOOH* · and form a stable complex.

Step1:

$$SO_3^{2-} + h\nu \rightarrow SO_3^{\cdot -} + e_{aq}^{\cdot -} \quad (8)$$

$$SO_3^{2-} + e_{aq}^{\cdot -} \rightarrow H^{\cdot} + SO_3^{\cdot -} \quad (9)$$

$$H^{\cdot} + H_2O \rightarrow H_3O^+ + e_{aq}^{\cdot -} \quad (10)$$

$$H^+ + e_{eq}^{\cdot -} \rightarrow H^{\cdot} \quad (11)$$

$$SO_3^{-\cdot} + O_2 \rightarrow SO_5^{-\cdot} \quad (12)$$

$$SO_3^{-\cdot} + H^+ \rightarrow HSO_3^- \quad (13)$$

$$SO_5^{-\cdot} + HSO_3^- \rightarrow SO_4^{2-} + SO_4^{-\cdot} + H^+ \quad (14)$$

$$SO_4{-\cdot} + H_2O \rightarrow SO_4^{2-} + HO^{\cdot} + H^+ \quad (15)$$

$$HSO_3^- + HO^{\cdot} \rightarrow H_2O + SO_3^{-\cdot} \quad (16)$$

$$CrO_4^{2-} + SO_3^{\cdot -} \rightarrow CrSO_4 \text{ (S-Cr)} \quad (17)$$

Step2: Where MnOOH· is a reactive hydroxyl group on the manganese oxide surface and the $2MnO_2$.CrOOH is a surface complex. Also, radical chain reactions can occur in medium reaction (Kuo et al., 2006, Xu et al., 2016a,b).

$$2MnO_2 + 2H^{\cdot} \rightarrow 2\ MnOOH^{\cdot} \quad (18)$$

$$MnOOH^{\cdot} + CrSO^- \rightarrow 2MnO_2\ .CrOOH \quad (19)$$

$$SO_3^{-\cdot} + O_2 \rightarrow SO_5^{-\cdot} \quad (20)$$

$$SO_3^{-\cdot} + H^+ \rightarrow HSO_3^- \quad (21)$$

$$SO_5^{-\cdot} + HSO_3^- \rightarrow SO_4^{2-} + SO_4^{-\cdot} + H^+ \quad (22)$$

$$SO_4{-\cdot} + H_2O \rightarrow SO_4^{2-} + HO^{\cdot} + H^+ \quad (23)$$

$$HSO_3^- + HO^{\cdot} \rightarrow H_2O + SO_3^{-\cdot} \quad (24)$$

At lower pH, HSO_3^- as the dominant ion can produce ·H as a weak reducing agent by either direct photolysis (Eq. (25)) or in the reaction of e_{aq}^- and H^+ (Eq. (11)) (Yu et al., 2019).

$$HSO_3^- + h\upsilon \rightarrow H^{\cdot} + SO_3^{-\cdot} \quad (25)$$

Also, at higher pH, almost all sulfur species are present as SO_3^{2-}, meaning that e_{aq}- and SO_3^-· are the predominant reducing radicals (Eq. (8)) (Cao et al., 2021). It is important to note that the performance of strong species including e_{aq}— and ·H with the potential −2.9 V and −2.3 V. Therefore, low pH is not suitable for this process. On the other hand, at high pH, production of oxidizing radicals can disrupt the process. According to the Fig. 2 r_{obs} of different process shows that the UV/S/M with 32 mg/L.min, UVS about 8.2 mg/L.min, and UV/Mn 5.97 mg/L.min are proved. In a study conducted by Yu et al. on the efficiency and mechanism of diclofenac degradation by the advanced UV/Sulfite reduction process, the effect of pH on diclofenac degradation at pH 3 to 11 was investigated, and pH 7 was optimal pH. By increasing the pH from 6.0 to 10 the constant reaction rate for diclofenac degradation decreased from 0.2294 to 0.1303 min^{-1}. Also, they proved that direct photolysis, k_{obs} is pH independent, and the values of k_{obs} 0.0743 min^{-1}, min^{-1} 0.0795 and min^{-1} 0.0720 are proved at pH 6, 7 and 9, respectively. This study proves that the effect of pH on DCF degradation is mainly due to radical reactions, not direct photolysis (Yu et al., 2019). In addition, Cr (VI) depletion is increased in the presence of several complexing agents including sulfite, citrate, EDTA, and humic acid. The positive effect of this substance is due to their ability to complexes with Cr (III) (Cao et al., 2021).

3.1.2. Reactive species identification in Cr photo- sedimentation

To gain further insight into the oxidation mechanism in the UV/sulfite/Manganese dioxide process, we investigated the pres-

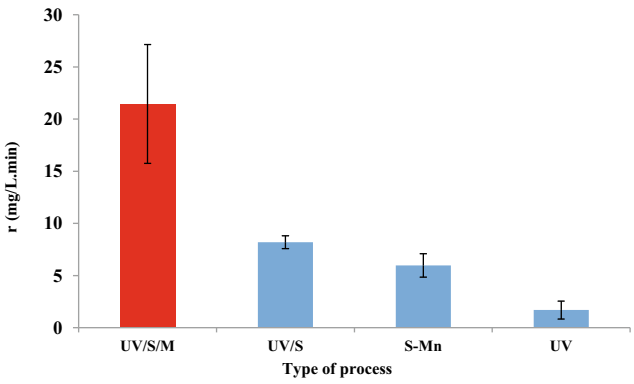

Fig. 2. Reaction rate of different processes of Cr photo- sedimentation at various initial pH values.

ence of different reactive species at different pH by Scavengers to explore of reactive species nature at pH 3, 7 and 11. Inspection of Fig. 3 shows that the contribution of reactive species at pH 7 with best performance about 45% and 55% of reaction species were reduction and oxidative species respectively. On the other hand at pH 11, about 95% of reaction species were oxidative species. This shows that reductive agents are important effective species to prepare Cr-S to formation complex with MnO_2 particle. At pH 7, a significant difference is observed, probably due to the low percentage of soluble sulfite as well as the presence of sulfate radical in reaction medium and formation ·OH radicals at this pH. ·OH radicals can be a scavenger to ·H radicals and other reductive agents (Rinklebe et al., 2016).

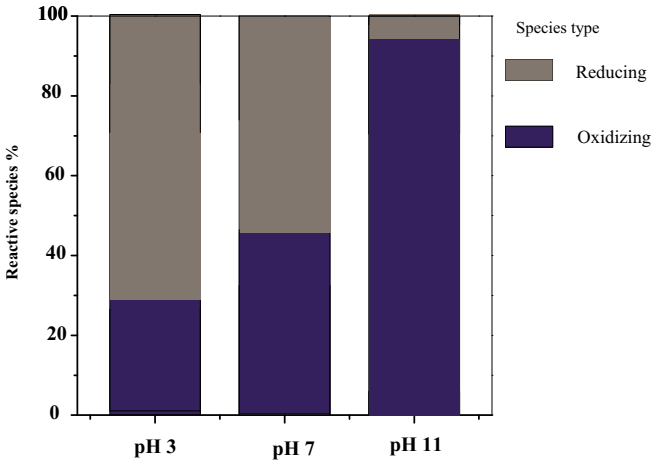

Fig. 3. Contribution of different reactive species in Cr photo- sedimentation at various initial pH values.

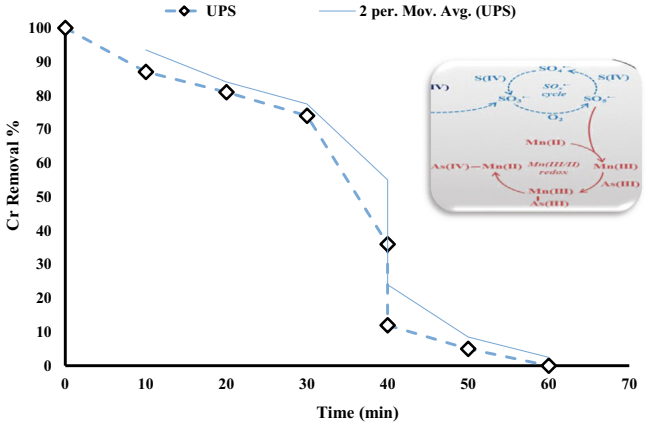

Fig. 4. Effect of time at high Cr levels. Initial conditions: pH 7, [Cr (III) = 10 mg L^{-1}, [MnO_2] = 1 mM, [Na_2SO_3] 0.4 mM.

3.1.3. Effect of different sulfite dose

Different amounts of sulfite were used to investigate the effect of sulfite dosage on Cr (III) removal at pH 3, 7 and 11) in optimal condition and fixed MnO_2 dose at 1 mM. C/C_o values decrease initially with the increase in sulfite dosage, reached a maximum value at 0.4 mM, and then decreased. According to Eqs. (13)–(23), sulfite can cause chain reactions that produce sulfur oxy and HO radicals, and increasing the sulfite concentration can improve the initial oxidation rate. However, they can react with sulfite by over-increasing the produced radicals $SO_4^{\cdot-}$ and HO· when used at much higher concentrations.

3.2. Sequential addition of Manganese dioxide

After 4 min of reaction time MnO_2 is added to the reaction solution, respectively (Fig. 4). In general, the rate of Cr-S complex formation and excess MnO_2 showed higher efficiency in Cr oxidation. In fact, sulfite is not recyclable because it is irreversibly converted to sulfate. Therefore, additional MnO_2 is required to promote sequential treatment. In the sequential addition of MnO_2, excess Cr (III) oxidation may be induced by the UV/Sulfite/MnO_2 process.

3.3. Kinetics and energy- economic evaluation in the photo-sedimentation process

In cost-effective factors, energy consumption is a limiting factor in the use of $AORP_s$ process. In this study kinetic and IUPAC methods were used to calculate photo-process energy consumption. The calculated of R^2 (0.95) in Table 1 indicate the fact that the Cr photo-sedimentation process follows the Pseudo first-order (PFO) kinetics. The values of R^2 are given in Table 1 and are calculated according to Fig. 5. The reaction rate increased with increasing concentration, which is due to the oxidizing and reducing species colliding with Cr and sediment formation. Because of need to more time or insufficient generate of reactive species to sedimentation of Cr in high concentrations so, the reaction rate decreased at a con-

Table 1
The PFO kinetics and electrical energy used in in different photo-reactor.

Process			Photo-degradation-PFO				
	Cr (mg L^{-1})	R^2	K_{obs} (min^{-1})	r_{obs} (mg/L.min)	Kinetic E_{EO} (kwh//m3)	figure-of-merit E_{EO} (kwh /m3)	TCS ($ g^{-1})
UV	50	0.9793	0.0748	3.74	125.23	119.6–107.41	18.75
	100	0.9647	0.0518	5.18	78.61	70.26–76.15	11.79
	250	0.9832	0.0218	5.45	65.37	63.24–68.12	9.80
UV/M	50	0.9761	0.1258	6.29	51.48	50.66–57.25	8.75
	100	0.9853	0.0825	8.25	41.27	0.26–43.1537	7.01
	250	0.9722	0.0672	16.80	33.82	31.24–36.12	5.74
UV/S	50	0.9763	0. 1671	8.355	35.76	92.23–97.54	5.72
	100	0.9963	0.0905	9.05	28.54	20.14–32.16	4.56
	250	0.9756	0.0673	16.82	9.47	8.24–11.02	1.51
UV/S/M	50	0.9946	0.5337	26.68	16.14	21.67–29.69	2.74
	100	0.9652	0.3269	32.69	10.22	16.26–21.74	1.73
	250	0.9765	0.1837	45.92	3.25	4.28–6.18	0.55

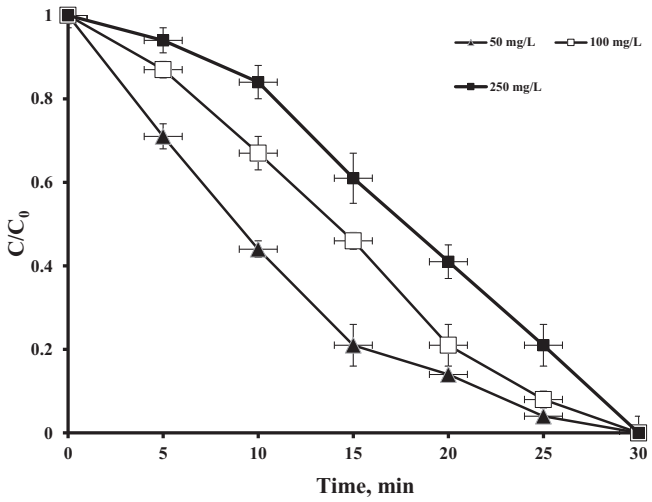

Fig. 5. C_t/C_o versus t to calculate reaction rate constant (conditions: $[MnO_2]$ = 0.1-mM, $[Na_2SO_3]$ = 0.4 mM).

centration of 250 mg L^{-1}. In Kinetic and IUPAC methods, energy consumption has increased with increasing Cr concentration, which according to the formula is clear that more Cr sedimentation at higher concentrations requires more energy. Also, the proximity of the energy obtained by the kinetic method in the range of energy obtained from the IUPAC method, which indicates the accuracy of the calculations. Constant reduction and reaction rate was probably due to the lower chance of Cr colliding with reactive species or insufficient generation of reactive species to sediment of high Cr concentrations. It leads to a decrease in the efficiency of the sedimentation process and as a result, the constant and reaction rate are reduced (Rastogi et al., 2009). Also, the amount of energy consumed decreases from 16.14 to 3.25 kWh per cubic meter, K_{obs} (min^{-1}) 0.5337 to 0.1837 and r_{obs} (mg/L.min) increase from 26.68 to 45.92. Because the amount of energy consumed varies depending on the concentration of the pollutant. In many studies, energy consumption increases with increasing pollutants, but in some studies it is quite the opposite and the amount of energy consumption decreases with increasing pollutant concentration (Moussavi et al., 2015; Xiao et al., 2017). Total cost of the system (TCS) was investigated at different concentrations. As shown in Table 1, the total cost of the MN process is much lower than other methods. In the UV, UVM, UVS, and USM methods, the total cost were estimated 9.80–18.75, 5.74–8.75, 5.72–1.51, and 2.74–0.55 $ when the Cr concentration increase 100 to 250 mg L^{-1}, respectively.

3.4. Sludge investigation

To investigate the sludge produced in the process, a concentration of 1000 mg L^{-1} chromium was used for 1–5 min reaction time. As shown in Fig. 6, over time, the amount of chromium removed increases and more sludge is produced. FTIR analyses was performed on the obtained sludge. As shown in Fig. 7 the broad band at 3450 cm^{-1} was observed in the spectra of all samples ascribed to surface hydroxyl groups and adsorbed water molecules. Pure MnO_2

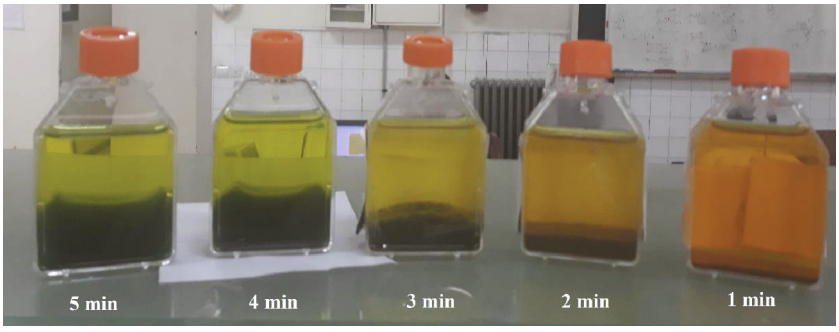

Fig. 6. The generated sludge in different reaction time of USM.

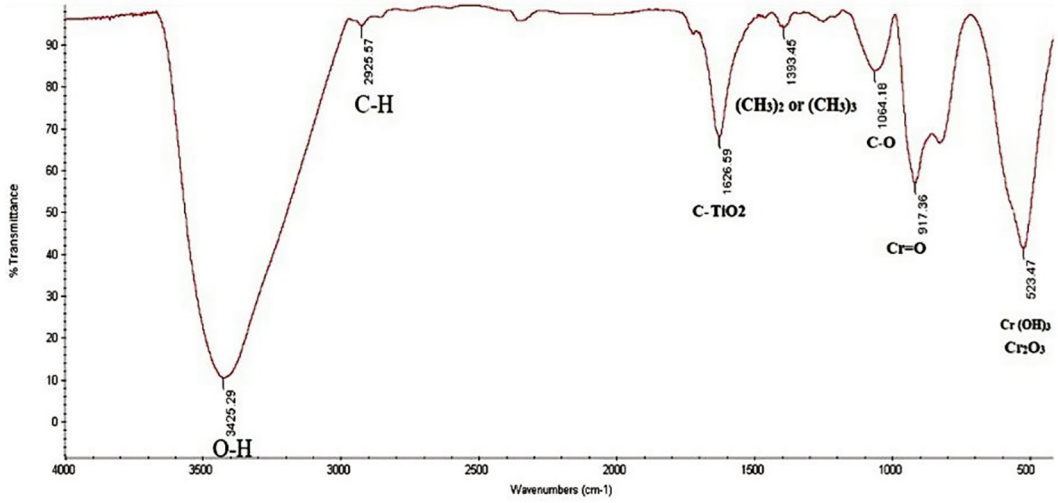

Fig. 7. The FTIR of generated sludge in USM process.

Table 2
Chemical parameters of real sample before and after the photo-sedimentation.

Parameters	Row water	After MnO_2 addition	UV/SO_3^-
pH (unit)	7.77	7.26	7.13
Cr (μg L^{-1})	273	89.75	3.26
HCO_3^- (mg L^{-1})	97.36	94.17	90.65
CO_3^{2-} (mg L^{-1})	65.17	44.87	43.59
NO_2^- (mg L^{-1})	14.18	10.65	7.38
Cl^- (mg L^{-1})	84.23	64.78	63.25
SO_4^{2-} (mg L^{-1})	51.94	126.34	87.16
HPO_4^{2-} (mg L^{-1})	10.27	8.63	2.58

Table 3
Comparison of different catalytic methods with the present method.

processes	Concentration of Cr	Reactive Concentration	pH	Time (min)	Performance	References
UV/H_2O_2/Fe^0/S_2O_8	10 mg L^{1}	H_2O_2/Fe^0 molar ratio, 2.0; S_2O_8, 0.75 mM L^{-1}	3	4	100%	(Yazdanbakhsh et al., 2020)
UV/TiO_2/Formate	30 mg L^1	TiO2: 10 mg L^{1}, Formate: 6 mg L^{1}	8	150	60%	(Massoudinejad et al., 2020)
Visible/pristine TiO_2	10 mg L^1	TiO_2 dosage (anatase) = 0.5 g L^1	5.36	50	100%	(Sun et al., 2021)
Sunlight/N, S-codoped Carbon Dot	100 mg L^1	0.5 mg.mL^{-1}	7.4	350	98%	(Saini et al., 2020)
Present study	100 mg L^1	[MnO_2] = 1 mM, [Na_2SO_3] 0.4 mM	6	6	%90	

nanoparticles have characteristic IR peaks at 1626 cm^{-1} corresponding to the bending vibrations of O–H groups. Furthermore, two peaks were observed in FTIR spectra of Cr at 1064 and 917 cm^{-1} for Cr–O and Cr=O, respectively. This is supported by new peaks in FTIR spectra of Cr (VI) 523 cm^{-1}, suggesting the formation of Cr $(OH)_3$ and, also the peak at 576 $cm^{-1}$was associated with the stable Cr_2O_3.

3.5. The impact of anion in real sample on Cr photo-sedimentation

Common anions in water and wastewater interfere with AORPs and reduce their effectiveness. The amount of water ions may also change after $AORP_s$ processes, especially photo-sedimentation. To explore the USM process application for treatment of Cr contaminated water, experiments in tow water matrix, including distillated and underground water (real sample) were carried out and the results were presented in Table. 2. Obviously, the USM process effectively removed Cr from different water matrix and all Cr concentrations were reduced to a value less than 273 μg L (the maximum permissible Cr level) after 1 min of USM process, Suggesting the great potential of the USM process on practical applications for Cr removal. The ions increase the time to reach the standard from 1 to 2 min as when the actual sample is applied. The increase in time can be due to three reasons:

Reaction of ions in water and production of weak radicals

a. Absorption of UV irradiation on the surface of the liquid and not reaching it to a greater depth
b. Ions such as phosphate can replace Cr in the process and disrupt the production of radical's cycles and may inhibit Cr oxidation by affecting the oxidative agents' process (Azarpira et al., 2019; Azizi et al., 2021).

As can be seen in Table 3 for comparing different catalytic methods with the present method, the present method has many advantages. These include less time, higher efficiency, less use of reactive materials, and no need for large pH changes. Also, sulfite and sulfate are completed with Manganese dioxide particles and therefore are not released into the environment.

4. Conclusions

In this study, removal of Cr in a novel process includes reduction and complexion, adsorption and oxidation in a UV/Sulfite/Manganese dioxide investigated. Information shows that the UV/S/M is very rapid process against other process (About twice as much UV/Mn and about six times much more than UV/S. Comparison of different catalytic methods prove that the USM process less time, higher efficiency, less use of reactive materials, and no need for large pH changes. This method investigated in a real well sample with anions, and more effective anions were Phosphate and Sulfate. Phosphate reacts with e_{aq}^- and react with sulfite radical and does not allow the formation of complexes, on the other hand Sulfate help to convert Cr^{+6} to Cr^{+3} and direct removal.

Funding

This research did not receive any specific grant from funding agencies in the public, commercial, or not-for-profit sectors.

Declaration of Competing Interest

The authors declare that they have no known competing financial interests or personal relationships that could have appeared to influence the work reported in this paper.

References

ALAH ABADI, A., Tabasi, A., Rastegar, A., et al., 2021. Removal of Acetaminophen from Aqueous Solutions by H2O2 + UV in the Presence of Zinc Oxide Nanoparticles Using Response Surface Methodology wastewater treatment. J Res. Environ Health 7, 105–119. https://doi.org/10.22038/JREH.2021.58231.1433.

Alam, U., Shah, T.A., Khan, A., et al., 2019. One-pot ultrasonic assisted sol-gel synthesis of spindle-like Nd and V codoped ZnO for efficient photocatalytic degradation of organic pollutants. Sep. Purif. Technol. 212, 427–437.

Azarpira, H., Abtahi, M., Sadani, M., et al., 2019. Photo-catalytic degradation of Trichlorophenol with UV/sulfite/ZnO process, simultaneous usage of homogeneous reductive and heterogeneous oxidative agents generator as a new approach of Advanced Oxidation/Reduction Processes (AO/RPs). J. Photochem. Photobiol., A 374, 43–51.

Azizi, S., Sarkhosh, M., Najafpoor, A.A., et al., 2021. Degradation of Codeine Phosphate by simultaneous usage of eaq− and •OH radicals in photo-redox processes: Influencing factors, energy consumption, kinetics, intermediate products and degradation pathways. Optik 167415.
Babu, D.S., Srivastava, V., Nidheesh, P., et al., 2019. Detoxification of water and wastewater by advanced oxidation processes. Sci. Total Environ. 696, 133961.
Cao, Y., Qiu, W., Li, J., et al., 2021. Review on UV/sulfite process for water and wastewater treatments in the presence or absence of O2. Sci. Total Environ. 765, 142762.
Dhaka, S., Kumar, R., Lee, S.-H., et al., 2018. Degradation of ethyl paraben in aqueous medium using advanced oxidation processes: efficiency evaluation of UV-C supported oxidants. J. Cleaner Prod. 180, 505–513.
Ding, K., Zhou, X., Hadiatullah, H., et al., 2021. Removal performance and mechanisms of toxic hexavalent chromium (Cr (VI)) with ZnCl2 enhanced acidic vinegar residue biochar. J. Hazard. Mater. 420, 126551.
Gekko, H., Hashimoto, K., Kominami, H., 2012. Photocatalytic reduction of nitrite to dinitrogen in aqueous suspensions of metal-loaded titanium (IV) oxide in the presence of a hole scavenger: an ensemble effect of silver and palladium co-catalysts. Phys. Chem. Chem. Phys. 14 (22), 7965–7970.
Hao, L., Wang, N., Wang, C., et al., 2018. Arsenic removal from water and river water by the combined adsorption-UF membrane process. Chemosphere 202, 768–776.
Harper, T.R., Kingham, N.W., 1992. Removal of arsenic from wastewater using chemical precipitation methods. Water Environ. Res. 64 (3), 200–203.
He, D., Xiong, Y., Wang, L., et al., 2020. Arsenic (III) removal from a high-concentration arsenic (III) solution by forming ferric arsenite on red mud surface. Minerals 10 (7), 583.
Kong, L., Hu, X., Peng, X., et al., 2020. Specific H2S release from thiosulfate promoted by UV irradiation for removal of arsenic and heavy metals from strongly acidic wastewater. Environ. Sci. Technol. 54 (21), 14076–14084.
Kong, L., Wang, Y., Hu, X., et al., 2021. Improving removal rate and efficiency of As (V) by sulfide from strongly acidic wastewater in a modified photochemical reactor. Environ. Technol., 1–25
Kuo, D.T., Kirk, D.W., Jia, C.Q., 2006. The chemistry of aqueous S (IV)-Fe-O2 system: state of the art. J. Sulfur Chem. 27 (5), 461–530.
Lee, C.-G., Alvarez, P.J., Nam, A., et al., 2017. Arsenic (V) removal using an amine-doped acrylic ion exchange fiber: kinetic, equilibrium, and regeneration studies. J. Hazard. Mater. 325, 223–229.
Lee, C.-G., H. Javed, D. Zhang, et al., 2018. Porous electrospun fibers embedding TiO2 for adsorption and photocatalytic degradation of water pollutants. Environ. Sci. Technol.
Liu, B., Kim, K.-H., Kumar, V., et al., 2020. A review of functional sorbents for adsorptive removal of arsenic ions in aqueous systems. J. Hazard. Mater. 388, 121815.
Liu, W., Yu, Y., 2021. Removal of recalcitrant trivalent chromium complexes from industrial wastewater under strict discharge standards. Environ. Technol. Innovation 101644.
Massoudinejad, M., Zarandi, S.M., Amini, M.M., et al., 2020. Enhancing photo-precipitation of chromate with carboxyl radicals: Kinetic, energy analysis and sludge survey. Process Saf. Environ. Prot. 134, 440–447.
Moussavi, G., Jiani, F., Shekoohiyan, S., 2015. Advanced reduction of Cr (VI) in real chrome-plating wastewater using a VUV photoreactor: Batch and continuous-flow experiments. Sep. Purif. Technol. 151, 218–224.
Ozcelik, E., Mercan, E.S., Erdemir, S., et al., 2021. Calixarene-tethered textile fabric for the efficient removal of hexavalent chromium from polluted water. Colloids Surf., A: Physicochem. Eng. Aspects 127045.
Rasolevandi, T., Naseri, S., Azarpira, H., et al., 2019. Photo-degradation of dexamethasone phosphate using UV/iodide process: Kinetics, intermediates, and transformation pathways. J. Mol. Liq. 295, 111703.
Rasolevandia, T., Azarpirab, H., Mahvia, A.H., 2020. Modeling and optimizing chromate photo-precipitation with iodide exciting under UV irradiation. Desalin. Water Treat. 195, 369–376.
Rastogi, A., Al-Abed, S.R., Dionysiou, D.D., 2009. Sulfate radical-based ferrous–peroxymonosulfate oxidative system for PCBs degradation in aqueous and sediment systems. Appl. Catal. B 85 (3–4), 171–179.
Rinklebe, J., Knox, A.S., Paller, M., 2016. Trace Elements in Waterlogged Soils and Sediments. CRC Press.
Sadani, M., Rasolevandi, T., Azarpira, H., et al., 2020. Arsenic selective adsorption using a nanomagnetic ion imprinted polymer: Optimization, equilibrium, and regeneration studies. J. Mol. Liq. 317, 114246.
Saini, D., Kaushik, J., Garg, A.K., et al., 2020. N, S-codoped carbon dots for nontoxic cell imaging and as a sunlight-active photocatalytic material for the removal of chromium. ACS Appl. Bio Mater. 3 (6), 3656–3663.
Sarkhosh, M., Sadani, M., Abtahi, M., et al., 2019. Photo-biological degradation of Bisphenol A, UV/ZnO/Iodide process at the center of biological reactor. J. Photochem. Photobiol., A 374, 115–124.
Sun, Y., Xu, L., Jin, P., et al., 2021. Simultaneous removal of colorless micropollutants and hexavalent chromium by pristine TiO2 under visible light: An electron transfer mechanism. Chem. Eng. J. 405, 126968.
Syam Babu, D., Nidheesh, P., 2021. A review on electrochemical treatment of arsenic from aqueous medium. Chem. Eng. Commun. 208 (3), 389–410.
Xiao, Q., Yu, S., Li, L., et al., 2017. An overview of advanced reduction processes for bromate removal from drinking water: Reducing agents, activation methods, applications and mechanisms. J. Hazard. Mater. 324, 230–240.
Xu, J., Ding, W., Wu, F., et al., 2016a. Rapid catalytic oxidation of arsenite to arsenate in an iron (III)/sulfite system under visible light. Appl. Catal. B 186, 56–61.
Xu, Y., Lin, Z., Zhang, H., 2016b. Mineralization of sucralose by UV-based advanced oxidation processes: UV/PDS versus UV/H2O2. Chem. Eng. J. 285, 392–401.
Yazdanbakhsh, A., Aliyari, A., Sheikhmohammadi, A., et al., 2020. Application of the enhanced sono-photo-Fenton-like process in the presence of persulfate for the simultaneous removal of chromium and phenol from the aqueous solution. J. Water Process Eng. 34, 101080.
Yu, X., Cabooter, D., Dewil, R., 2019. Efficiency and mechanism of diclofenac degradation by sulfite/UV advanced reduction processes (ARPs). Sci. Total Environ. 688, 65–74.
Zaw, M., Emett, M.T., 2002. Arsenic removal from water using advanced oxidation processes. Toxicol. Lett. 133 (1), 113–118.
Zhang, W., Zhang, G., Liu, C., et al., 2018. Enhanced removal of arsenite and arsenate by a multifunctional Fe-Ti-Mn composite oxide: photooxidation, oxidation and adsorption. Water Res. 147, 264–275.